Meeting of the Apical and Basolateral Endocytic Pathways of the Madin–Darby Canine Kidney Cell in Late Endosomes

Robert G. Parton, Kristian Prydz, Morgane Bomsel,‡ Kai Simons, and Gareth Griffiths

European Molecular Biology Laboratory, Cell Biology Program, Postfach 10.2209, D-6900 Heidelberg, Federal Republic of Germany and ‡ER64-Centre National de la Recherche Scientifique, Etats Liés Moléculaires, F-75006 Paris, France

Abstract. Electron microscopic approaches have been used to study the endocytic pathways from the apical and basolateral surface domains of the polarized epithelial cell, MDCK strain I, grown on polycarbonate filters. The cells were incubated at 37°C in the presence of two distinguishable markers administered separately to the apical or the basolateral domain. Initially each marker was visualized within distinct apical or basolateral peripheral endosomes. However, after 15 min at 37°C, both markers were observed within common perinuclear structures. The compartment in which meeting first occurred was shown to be a late endosome (prelysosome) that labeled extensively with antibodies against the cation-independent mannose-6-phosphate receptor (MPR) on cryosections. With increasing incubation times, markers passed from these MPR-positive structures into a common set of MPR-negative lysosomes that were mainly located in the apical half of the cell.

A detailed quantitative analysis of the endocytic pathways was carried out using stereological techniques in conjunction with horseradish peroxidase and acid phosphatase cytochemistry. This enabled us to estimate the absolute volumes and membrane surface areas of the endocytic organelles involved in apical and basolateral endocytosis.

SELECTED plasma membrane components of mammalian cells are continuously taken into the cell by endocytosis (Steinman et al., 1983; Goldstein et al., 1985). After 5 min at 37°C, internalized markers enter tubulovesicular elements, termed early or peripheral endosomes, before being routed to lysosomes or recycled back to the plasma membrane (Storrie, 1988; Courtoy, 1989; Gruenberg and Howell, 1990). Ligands destined for lysosomes pass from early endosomes to juxtanuclear late endosomes (Helenius et al., 1983; Hopkins, 1986), also referred to as prelysosomes (Kornfeld and Mellman, 1989), with kinetics that appear to depend on both the cell type and the ligand used (Hubbard, 1989). Late endosomes are enriched in both the cation-independent mannose-6-phosphate receptor (MPR)[1] and lysosomal proteins as compared with early endosomes (Geuze et al., 1988; Griffiths et al., 1988) and have been proposed to be the target of *trans*-Golgi network (TGN)-derived vesicles containing newly synthesized lysosomal enzymes on their way to lysosomes (Kornfeld and Mellman, 1989). Late endosomes are more acidic than both early endosomes (Schmid et al., 1989; Fuchs et al., 1989) and the TGN (Griffiths et al., 1988). The low pH may facilitate dissociation of lysosomal enzymes from MPRs, allowing the latter to recycle back to the TGN for further rounds of transport, while the lysosomal enzymes pass to lysosomes (Goda and Pfeffer, 1988). In agreement with this model is the finding that at later times endocytic markers reach MPR-negative structures containing lysosomal proteins; the latter are most likely functional lysosomes (Brown et al., 1986; Geuze et al., 1988; Griffiths et al., 1988).

In the polarized epithelial cell, where the surface membrane is divided into two domains of distinct composition, continual endocytosis and recycling also occur (Simons and Fuller, 1985). Moreover, there is extensive membrane traffic between the two domains (transcytosis) (Abrahamson and Rodewald, 1981; Limet et al., 1985; Hoppe et al., 1985; Mostov and Simister, 1985; von Bonsdorff et al., 1985). Despite this process, the cell maintains its polarity with high efficiency (Fuller and Simons, 1986).

We have studied endocytosis in polarized monolayers of MDCK cells grown on polycarbonate filters. In the preceding paper (Bomsel et al., 1989), it was shown that markers internalized from the two surface domains of the MDCK cell were initially located in distinct early endocytic structures but that meeting of the markers occurred within 15 min after the onset of internalization. In this study, we have characterized and quantitated the endocytic pathways from the apical and basolateral domains of the MDCK cell by an ultrastructural approach and have demonstrated that the two pathways meet in late endosomes (or prelysosomes) enriched in the MPR.

Materials and Methods

Cells

MDCK strain I cells were grown on 0.4-μm-pore polycarbonate filters

1. *Abbreviations used in this paper*: HRP, horseradish peroxidase; MPR, mannose-6-phosphate receptor; *Sv*, surface density; TGN, *trans*-Golgi network.

(Costar Corp., Cambridge, MA) for 3–4 d (Bomsel et al., 1989). The electrical resistance across the bilayer was routinely assayed as described previously (Fuller et al., 1984) and was always >2,000 $\Omega \cdot cm^2$.

Markers of Endocytosis

Cells were washed twice with the incubation medium (MEM, containing 0.2% BSA, 350 mg/liter Na HCO_3, and 10 mM Hepes). They were incubated for various times at 37°C or 20°C, in the incubation buffer with horseradish peroxidase (HRP, 10 mg/ml), added to the apical medium (Sigma Chemical Co., St. Louis, MO) and BSA-coated gold particles (OD_{520} ~20) in the basolateral medium. 13–14 nm gold was prepared by the tannic acid method (Slot and Geuze, 1985) and bound to 200 μg/ml BSA at pH 7.0.

Due to the relatively low endocytic rate from the apical surface of the MDCK cell (von Bonsdorff et al., 1985), colloidal gold-BSA did not give a sufficiently high signal when administered apically. For this reason, in those experiments in which HRP was applied basolaterally, a membrane marker was used to follow endocytosis from the apical surface. An anti-MDCK rabbit polyclonal antibody against MDCK strain II cells (a gift from J. Gruenberg, European Molecular Biology Laboratory) was bound to the apical cell surface (30 min on ice). After washing three times over 30 min, the cells were incubated with protein A-gold for 30 min on ice and then warmed to 37°C for various times while 10 mg/ml HRP was administered basolaterally. Alternatively, cationized ferritin (0.1 mg/ml; Sigma Chemical Co.) was bound to the apical surface (5 min on ice) and then warmed to 37°C for various times with HRP in the basolateral medium.

To terminate the incubations, cells were either fixed without a washing step or washed twice with ice-cold incubation buffer before fixation, as described below.

Electron Microscopy

Cells on polycarbonate filters were fixed with 1% glutaraldehyde in 0.1 M cacodylate buffer, pH 7.4 (cacodylate buffer) for 30 min. To visualize HRP, the fixed cells were rinsed with cacodylate buffer, incubated in cacodylate buffer containing 0.1% diamino-benzidine (DAB; Sigma Chemical Co.) for 1 min and then H_2O_2 was added to a final concentration of 0.01% to initiate the reaction. After a 2-min incubation in the dark, the DAB solution was removed and the cells were washed with cacodylate buffer (Marsh et al., 1986). The cells were postfixed for 60 min in 1% OsO_4 containing 1.5% potassium ferricyanide, or with 2% aqueous OsO_4 and block-stained for 1 h with 1% uranyl acetate in 50 mM maleate buffer, pH 5.2. Cells were dehydrated in an alcohol series, and embedded in Epon. Sectioning was performed perpendicular to the plane of the filter to obtain vertical sections as required for the stereological analysis. The cells showed no endogenous peroxidase activity.

Acid phosphatase was visualized by the lead capture method as described previously (Griffiths et al., 1983*b*) with a 75-min incubation with the reaction mixture. When the same sample was to be stained for acid phosphatase and HRP, the staining for acid phosphatase was performed before the staining with DAB.

Morphometric Analysis

Mean Cell Volume. The absolute volume of the MDCK I cell was estimated by measuring the mean area of filter covered by one cell (124 μm^2) and the mean cell height (9.38 μm) across the monolayer (Griffiths et al., 1984, 1989*b*). The former was estimated by counting the number of cells per area of filter on light micrographs after staining the nuclei with Hoechst dye, and the latter was measured as outlined below.

Stereology. For all the sterological analysis Epon blocks were sectioned perpendicular to the plane of the filter to obtain the necessary vertical sections (Baddeley et al., 1986). Photographs were taken at three different magnification levels as described below and all the measurements were made on negatives enlarged 4.1 times on an EMBL-designed projector system.

The three magnification levels used were as follows: Level 1: a primary magnification of 2,800× was used to gain estimates for several morphological features of the MDCK I cell. Sections were cut from a total of six Epon blocks after embedding two filters of MDCK I cells. 35 random micrographs were taken along the monolayer by using the translation controls of the microscope.

The surface to volume ratio (*Sv*) of the MDCK I cell was estimated using the method of Baddeley et al. (1986). A cycloid lattice grid (Cruz-Orive and Hunziker, 1986) was laid over the projected negatives. Intersections of the cycloid with the apical, basal and lateral surface domains and the points over the cell were counted and *Sv* was calculated as described previously (Griffiths et al., 1989*b*).

The volume density of the cytoplasm (the ratio of the cytoplasmic volume to the cell volume) was estimated using the same negatives and a square double lattice grid to relate the number of points over the nucleus to the number of points over the cell. The mean cell height across the monolayer was directly measured on the same negatives at three different fixed positions across the negative.

Magnification level 2: a primary magnification of 10,500× was used to obtain estimates for the volume density of HRP or acid phosphatase-labeled compartments. 25–35 random micrographs were analyzed using a double-square lattice grid. Points over HRP or acid phosphatase-labeled structures were related to the points over the cytoplasm of the cell.

Magnification level 3: 20–30 micrographs were taken at a primary magnification of 33,000× after systematically searching for HRP or acid phosphatase-labeled structures. The *Sv* of the labeled structures was estimated by using square lattice grids of various sizes and relating the number of points over the structures of interest to the intersections the grid lines made with the limiting membrane. The *Sv* of these structures was calculated as described by Weibel (1979).

Cryomicrotomy and Immunolabeling

Filter-grown MDCK cells were processed for EM after fixation either as described above for plastic sections or alternatively in 1% glutaraldehyde in 250 mM Hepes, pH 7.4. After washing, the filters were cut into segments and incubated in 10% gelatin in PBS for 10 min at 37°C. Two pieces of filters were then laid on top of each other and the gelatin was allowed to set at 4°C. The gelatin was cross-linked with 8% paraformaldehyde in 250 mM Hepes, pH 7.4, for 1 h at room temperature. The samples were then mounted on copper stubs with the filter perpendicular to the plane of sectioning and sectioned on a ultramicrotome (model OMU4; Reichert, Vienna, Austria) with cryoattachment. Labeling was performed as described previously (Griffiths et al., 1983*a*, 1984). The affinity-purified anti-HRP was a gift from J. Gruenberg (European Molecular Biology Laboratory). The antiserum against chicken 215K cation-independent mannose-6-phosphate receptor was prepared by K. Römisch and B. Hoflack (European Molecular Biology Laboratory). This antiserum shows specificity only for the cation-independent MPR by immunoblotting of MDCK cell homogenates.

Results

Meeting of the Endocytic Pathways from the Two Surface Domains of MDCK Cells

HRP was administered independently to the two domains of MDCK I cells grown on polycarbonate filters. At early times of internalization (5–10 min at 37°C), apically administered HRP was visualized close to the apical surface of the cell, whereas basolateral HRP was observed in profiles along the lateral and basal surfaces. A similar distribution of HRP was shown by von Bonsdorff et al. (1985) and is in good agreement with the confocal microscopic observations of Bomsel et al. (1989). These peripheral structures correspond to the early endosomes described in the companion paper.

By EM the apical and basolateral early endosomes appeared morphologically similar (Fig. 1, *a*, *b*, and *d*). Both had tubular and vesicular portions as observed in other cells (Geuze et al., 1983; Marsh et al., 1986). HRP reaction product often appeared to be limited to the periphery of such structures and to surround an electron-lucent lumen (Fig. 1). Such images have been observed by other workers and assumed to represent spherical vesicles (Steinman et al., 1976; de Chastellier et al., 1987). However, in some of our images an inner membrane is visible (Fig. 1, *a* and *b*), suggesting that a tubule, or more likely, cisterna, containing HRP may surround an electron-lucent area. In addition to these structures, a small number of noncoated vesicles directly underly-

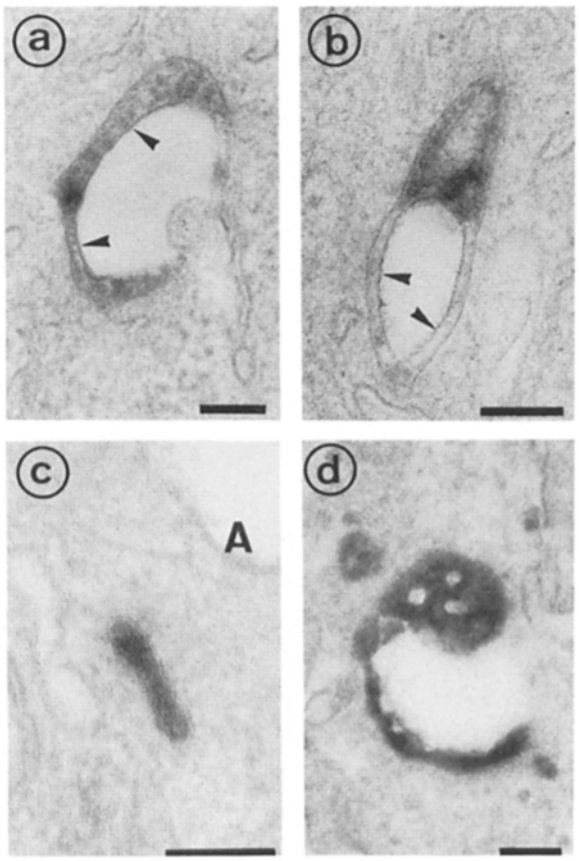

Figure 1. Early apical and basolateral endocytic structures in the MDCK cell. Examples of structures labeled with HRP after a 5-min apical (*a*, *b*, and *c*) or basolateral (*d*) incubation at 37°C. *a* and *b* show structures located in the apical region of the cell. HRP reaction product appears to be limited to a membrane-enclosed tubule or, more likely, cisterna whose inner membrane (*arrowheads*) encloses an electron-lucent lumen. *c* shows a typical small uncoated structure lying close to the apical surface of the cell (*A*). *d* shows a basolateral early endosomal structure. Again an electron-lucent area is surrounded by HRP reaction product. Bars, 0.1 μm.

ing the apical surface were labeled after short incubations with HRP in the apical medium (Fig. 1 *c*; see below).

With longer incubations at 37°C, HRP from the two surfaces appeared within perinuclear structures. To determine whether the pathways shared late endocytic compartments, two distinguishable markers were applied independently to the surfaces of the MDCK cell. BSA-gold was internalized from the basolateral surface and HRP from the apical surface of the cell. After continuous internalization of these markers for a period of 15 min or longer at 37°C, colocalization of HRP and colloidal gold was observed within profiles close to the nucleus (Fig. 2). No colocalization was observed in peripherally located structures lying close to the apical and basolateral surfaces of the cell.

To establish the precise kinetics of the meeting of the two pathways and define the compartment where meeting first occurred, HRP was internalized basally and membrane-bound gold was internalized apically. The use of HRP as a basolateral marker prevented any possible problems with access of a particulate marker along the lateral spaces to apical portions of the cell and gold bound to the apical membrane via an anti-MDCK antiserum provided the highest signal of all the markers used (results not shown). After 5–10 min internalization at 37°C, there was very little evidence of colocalization of the two endocytic markers within the same organelle. HRP and gold particles were predominantly located in peripheral structures lying close to the basolateral and apical surfaces, respectively (Fig. 3). However, after 15 min of internalization, colocalization of HRP and gold particles was apparent within structures predominantly in the supranuclear portion of the cell close to the Golgi stacks (Fig. 4). Identical results were obtained with cationized ferritin as a marker of the apical surface and HRP as a basolateral marker (see Fig. 5 *d*). These results are therefore in good agreement with the biochemical and confocal microscopic results presented in the companion paper (Bomsel et al., 1989). The organelles containing the two markers had numerous vesicular inclusions and resembled the multivesicular bodies previously described in these cells (von Bonsdorff et al., 1985) and in other cell types (McKanna et al., 1979; Wall et al., 1980; Hopkins and Trowbridge, 1983).

Further experiments were designed to test whether any meeting could be detected within early endosomes. The passage of ligands from endosomes to lysosomes is blocked at 20°C (Dunn et al., 1980; Marsh et al., 1983) and Griffiths et al. (1988) showed that this block occurs between peripheral early endosomes and an intermediate prelysosomal compartment (late endosome). We therefore investigated whether any meeting of apical and basolateral markers occurred at this temperature. No colocalization of the markers could be demonstrated despite the presence of gold labeled structures and HRP-labeled structures in close proximity (results not shown). These results confirm that MDCK cells possess distinct apical and basolateral early endosomes. Meeting occurs in a later compartment, after a lag >5–10 min at 37°C and subsequent to the 20°C block in the pathway.

Characterization of the Meeting Compartment

To characterize the compartment in which the basally applied and apically applied ligands colocalized, ultrathin frozen sections were prepared. The thawed sections were double-labeled with antibodies to HRP and to the cation-independent MPR.

Cryosections were prepared after a 15-min internalization of apically bound gold and basally administered HRP (see above), a 15-min internalization of apically bound cationized ferritin and basal HRP, or after a continuous incubation for 2 h at 37°C with BSA-gold in the basal medium and HRP in the apical medium. After 15 min at 37°C, gold internalized from the apical surface could be visualized within peripheral HRP-negative structures showing negligible labeling with anti-MPR antibodies (Fig. 5 *a*). Basolaterally internalized HRP was visualized within structures in close proximity to the lateral and basal surfaces (Fig. 5 *b*). Labeling for MPR was very low but consistently observed in these basolateral structures. In contrast, structures containing both the internalized gold and showing labeling for HRP were more heavily labeled with anti-MPR antibodies (Fig. 5 *c*). Similar results were obtained with the two other sets of markers. Cationized ferritin bound to the apical surface of the cell colocalized with basolateral HRP after 15 min at 37°C in MPR-enriched structures (Fig. 5 *d*). After a 2-h continuous incubation with

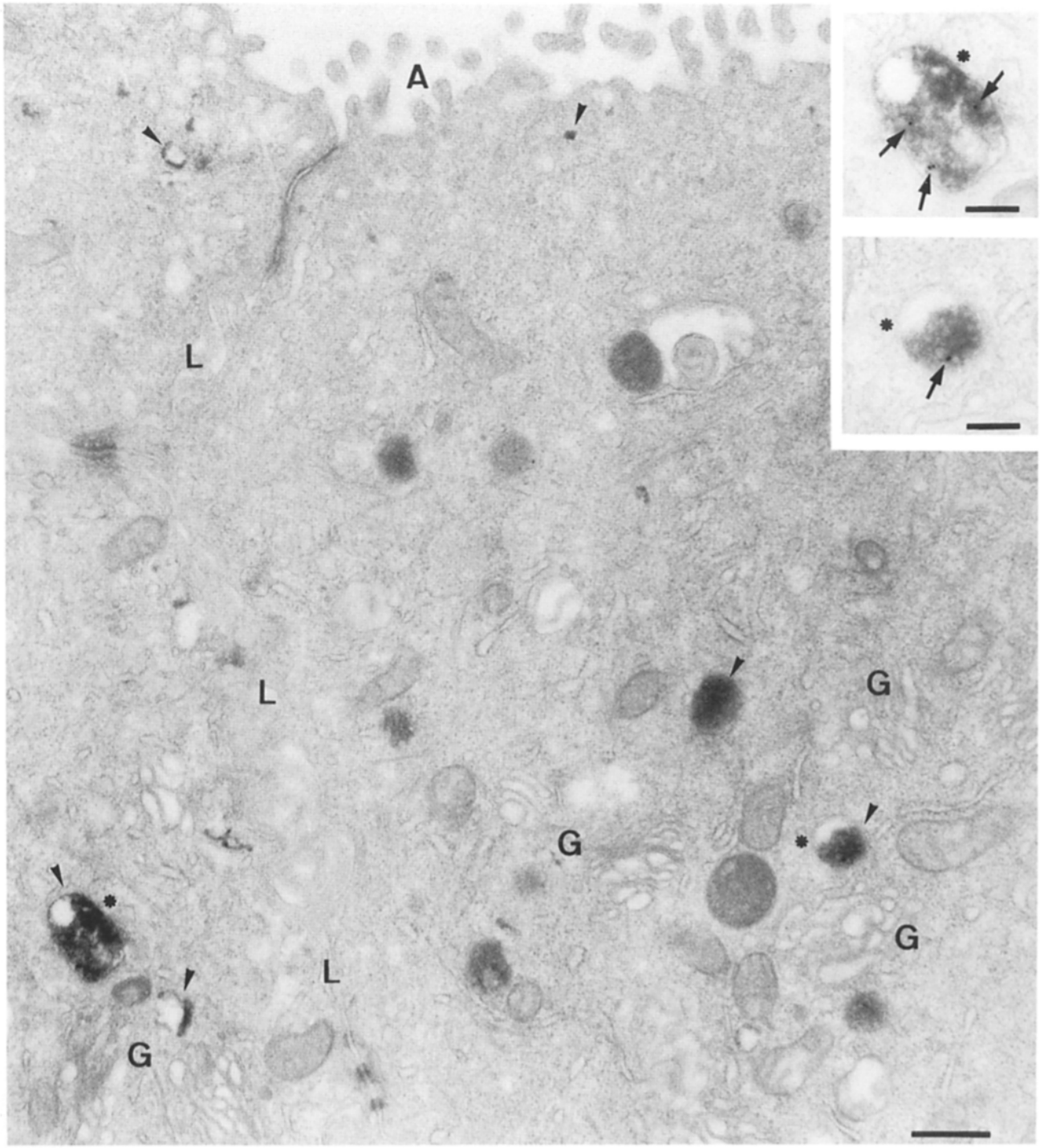

Figure 2. Meeting of apical and basolateral fluid-phase markers in the MDCK cell. MDCK cells were incubated with HRP apically and BSA-gold basolaterally for 2 h at 37°C. HRP is present in small structures under the apical surface and in larger structures deeper in the cell (*arrowheads*). HRP and gold particles colocalize in structures (*asterisks*) close to the Golgi stacks (*G*). Higher magnification views of these two structures showing the internalized gold particles (*arrows*) are shown in the insets. The multivesicular nature of the structures where meeting occurs is apparent. *A*, apical surface. *L*, lateral space. Bars, main figure, 0.5 μm; insets, 0.2 μm.

BSA-gold in the basolateral medium and HRP in the apical medium, meeting was again detected within structures that labeled extensively with the anti-MPR antibody (Fig. 5 *e*) but not within peripheral structures showing low labeling for MPR. The MPR-enriched organelles where meeting occurred varied in structure, often contained intralumenal tubulovesicular membranes, and were predominantly in a perinuclear location in the cell.

These results, using three different marker systems, have shown that MDCK cells possess two distinct sets of early en-

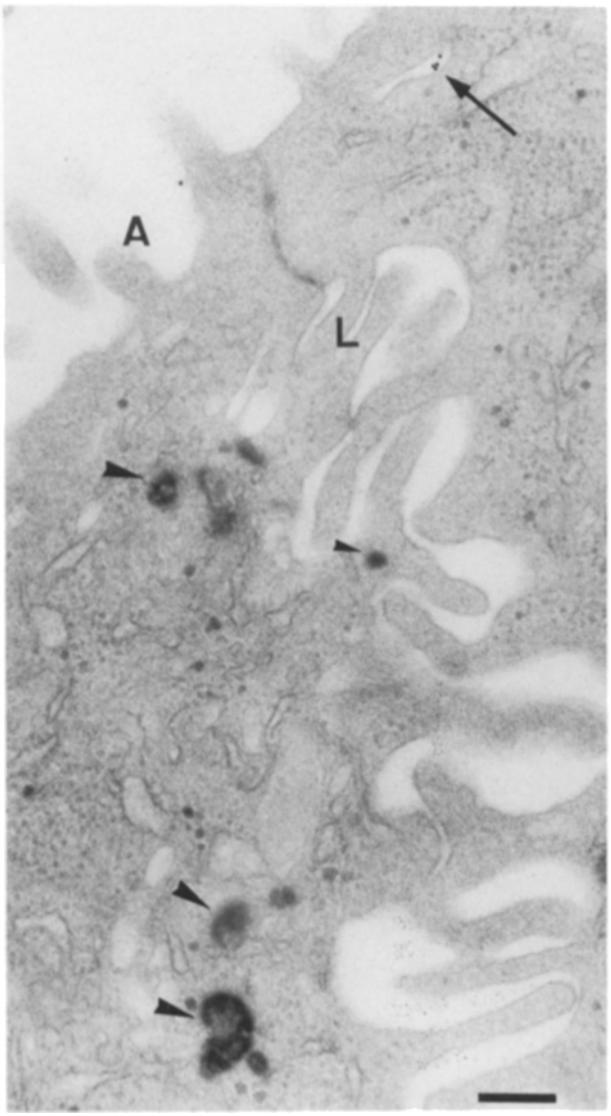

Figure 3. Distribution of apical and basolateral markers in the MDCK cell after 5 min at 37°C. Epon section of an MDCK cell fixed 5 min after the onset of internalization of apical membrane-bound gold and basolateral HRP. 9 nm protein A-gold was bound to the apical surface via an anti-MDCK antibody at 4°C. The cells were then warmed to 37°C for 5 min in the presence of basolateral HRP. Gold particles are apparent in a tubular structure underlying the apical surface (*arrow*), whereas HRP-labeled structures (*arrowheads*) lie close to the lateral space (*L*). A possible HRP-labeled coated vesicle is indicated by a small arrowhead. Note that some basolaterally labeled structures are located close to the apical surface (*A*). Bar, 0.2 μm.

dosomes showing low or negligible labeling for MPR and that markers from these compartments meet in MPR-enriched late endosomes (Kornfeld and Mellman, 1989).

Accumulation of Internalized Ligands within Putative Lysosomes

In nonpolarized cells ligands have been shown to be transported from MPR-containing endosome structures to MPR-negative lysosomes (Griffiths et al., 1988; Geuze et al., 1988). Therefore, we investigated whether ligands would pass from the late endosomes to MPR-negative structures in this cell type. For this analysis, BSA-gold was used as an easily quantifiable and nondegradable marker of bulk flow. Note that our aim was not to define the kinetics of this step of the pathway; BSA-gold appears to be slower in its movement to the end station of the endocytic pathway as compared with HRP (Bomsel et al., 1989).

BSA-gold was internalized from the basolateral surface of the cell for 40 min at 37°C and then the cells were washed and reincubated in ligand-free medium for 40 min, or overnight at 37°C. The 40-min incubation in ligand-free medium was used to chase the gold from early endosomes to late endocytic compartments, whereas the overnight incubation was intended to chase gold to the end station of the endocytic pathway.

We first determined the percentage of the internalized gold particles present in MPR-negative and MPR-positive structures after the two chase times by immunolabeling of frozen sections. As shown in Table I, after a 40-min chase, 75% of the total internalized gold was within MPR-positive structures (Fig. 6). After the overnight chase, however, the percentage of gold particles within the MPR compartment had decreased considerably and represented only 27% of the total internalized gold. The remainder of the gold particles was present in large aggregates in MPR-negative, electron-dense structures (Fig. 7), which we presume to be lysosomes.

To investigate in more detail the accumulation of gold within the lysosomes and to determine whether the marker reaches these organelles via the MPR-enriched late endosomes, we counted the absolute number of gold particles in the various compartments after the two incubation times.

The total number of gold particles within the cell after a 40-min uptake followed by a 40-min chase was approximately equal to that found in the cell after the overnight chase. This indicates that negligible exit of gold from the cells occurred during this period due, for example, to transcytosis or release of lysosomal contents. Using the absolute number of gold particles per cubed micron of cytoplasm, together with the results from the MPR labeling of frozen sections (above), we could show that the number of gold particles in the MPR-positive compartment decreased by ~2,300 per cell during the overnight chase, whereas gold in the MPR-negative compartment (lysosomes) increased by 2,600 gold particles per cell during the same time period. These results show clearly that most, if not all, of the gold particles that reach the lysosomes must pass through the late endosomes.

The labeled profiles after the overnight chase clearly had a greater mean number of gold particles than the structures labeled after the 40-min chase (Table I). As only half as many labeled profiles per cytoplasmic volume were observed after the overnight chase, this suggested that the gold particles were chased from a relatively large compartment to one of a smaller volume.

Our qualitative observations indicated that the location of the late endosomes and the lysosomes differed in that the latter are predominantly in the apical part of the cell whereas the former are found to be above and around the nucleus. We therefore counted the percentage of the internalized gold particles in the basal region of the cell (arbitrarily defined as below the midpoint of the nucleus). After the 40-min chase,

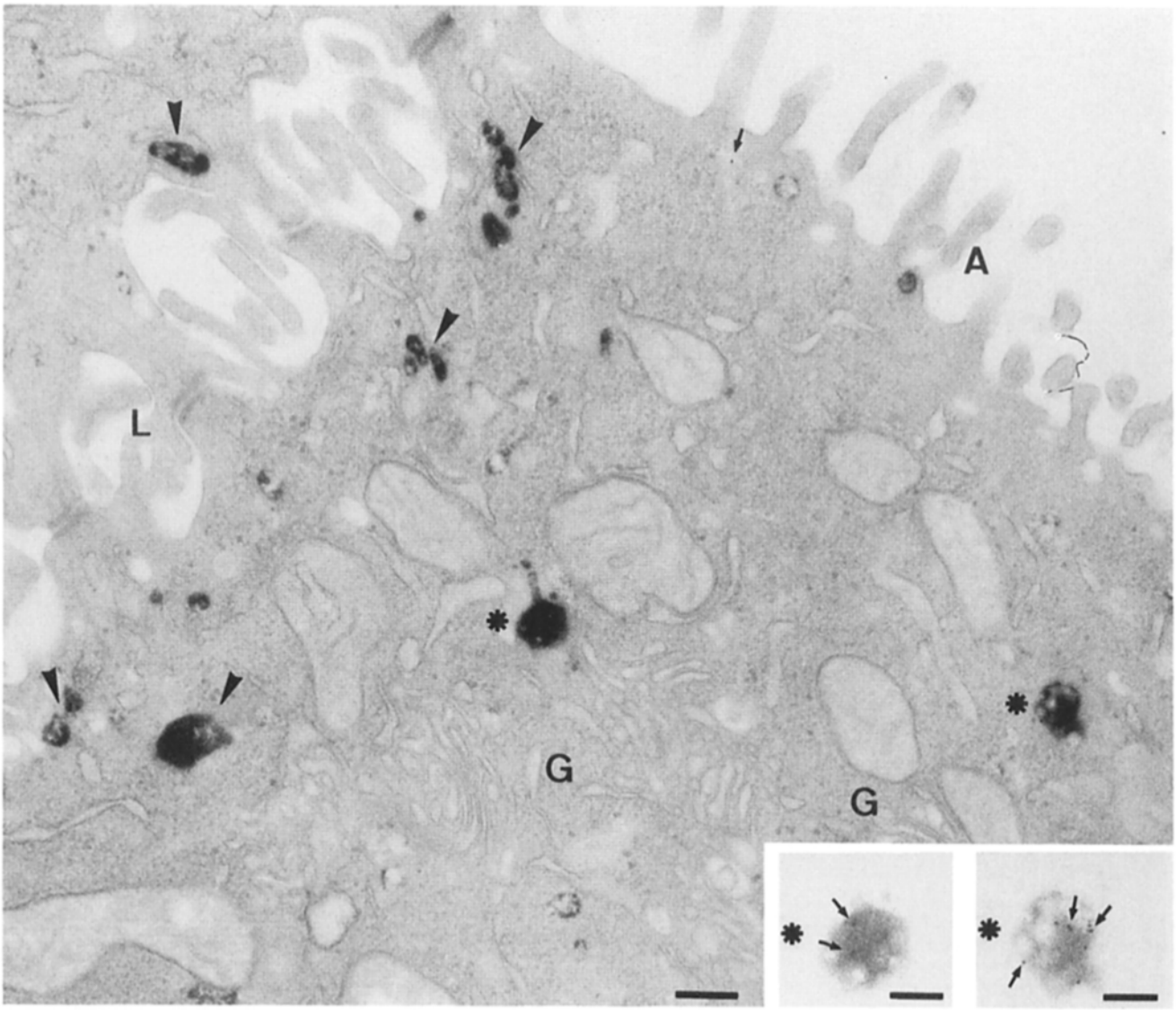

Figure 4. Meeting of apical and basolateral markers in the MDCK cell after 15 min at 37°C. Epon section of MDCK cell fixed 15 min after the onset of internalization of apical membrane-bound gold and basolateral HRP (for details see Fig. 3). HRP reaction product fills a number of vesicles (*arrowheads*) alongside the lateral space (*L*). Basolaterally administered HRP and apically applied gold colocalize in structures (*asterisks*) close to the Golgi area (*G*) of the cell as shown at higher magnification and with a lighter printing in the two insets (*arrows* indicate gold particles). A gold particle is also evident in an ill-defined structure (possibly a grazing section of a vesicle) underlying the apical surface (*arrow*). *A*, apical surface. Bars, main figure, 0.5 μm; insets, 0.1 μm.

~31% of the gold particles were present in the basal region. After the overnight chase, however, when the labeled structures were almost exclusively lysosomal by the criteria described above, only 4% of the gold particles were in basally located structures. Thus, in the MDCK cell the lysosomes are predominantly (or exclusively) located in the apical region of the cell, whereas the late endosomes are also found in basal regions.

Acid phosphatase has been shown to be present in the lysosomes and the late endosomes of normal rat kidney and baby hamster kidney cells but absent from early endosomes (Gruenberg et al., 1989; Griffiths, G., R. Matteoni, R. Back, and B. Hoflack, manuscript in preparation). We observed a similar distribution of this enzyme in the MDCK cell. Fluid-phase markers were observed in acid phosphatase–negative structures after short incubations at 37°C (5–10 min) but after longer incubations, passed into acid phosphatase–positive structures (Fig. 7). After the 40-min chase of BSA-gold, ~90% of the internalized gold particles were within acid phosphatase–positive structures and after the overnight chase this had increased to almost 100% (results not shown). Thus, both the MPR-enriched late endosomes and the lysosomes in MDCK cells contain detectable amounts of acid phosphatase.

Volume of the Endocytic Compartments in the MDCK Cell

To gain a quantitative view of the endocytic pathways in the MDCK cell, HRP was administered independently to each of the two surface domains and internalized for various times

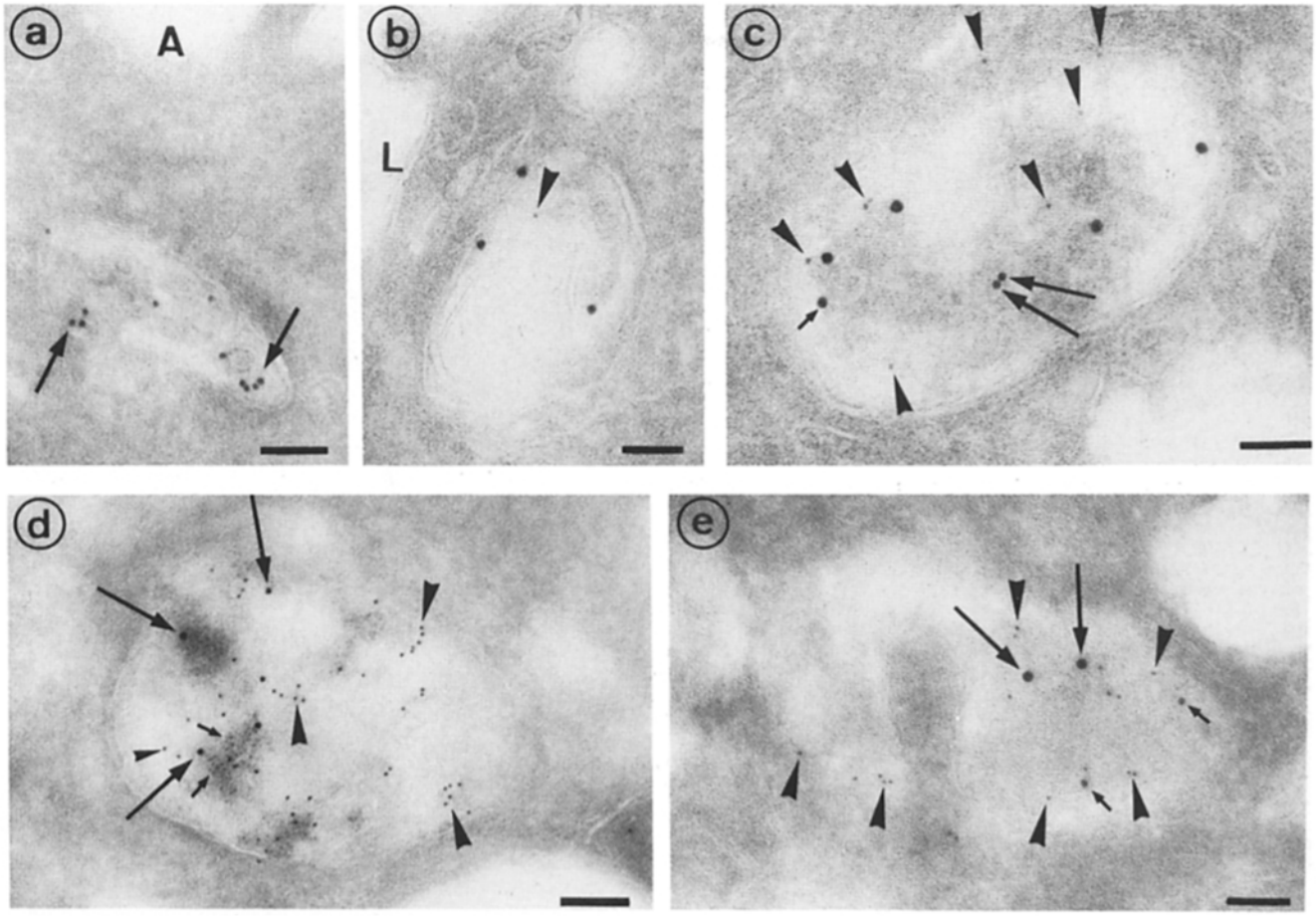

Figure 5. Characterization of compartments containing apically and basolaterally internalized markers on cryosections. Cryosections were double-labeled with antibodies to MPR and to HRP. Three different sizes of gold are shown in the figure; the largest gold (13–14 nm) corresponds to the basolaterally internalized marker, the medium-sized gold (9 nm) (or in Fig. 4, *d*, cationized ferritin) corresponds to the apically administered marker and the smallest (6 nm) represents labeling for MPR. *a*, *b*, and *c* show cryosections of cells after binding protein A-gold to the apical surface and internalization for 15 min at 37°C with HRP in the basolateral medium (see legend to Fig. 1). In *a*, gold (*arrows*) internalized from the apical surface (*A*) is evident within a putative early apical endosome, which shows no labeling with anti-HRP or anti-MPR. *b* shows a typical basolateral endosome, in close proximity to the lateral surface (*L*) which labels with anti-HRP (*large gold*) but has no apically internalized gold. This compartment shows low, but significant labeling with anti-MPR (small gold, *arrowhead*). *c* shows an example of a compartment where the basolateral marker (HRP, labeled with anti-HRP and 13 nm protein A-gold, *small arrows*) colocalizes with the apical marker (BSA-gold, 9 nm; *large arrows*). The compartment labels significantly with antibodies against the cation-independent mannose 6-phosphate receptor (6 nm gold, *arrowheads*). (*d*) Cationized ferritin was bound to the apical surface and internalized for 15 min at 37°C, with HRP in the basolateral medium. HRP (labeled with anti-HRP and large gold, *large arrows*) colocalizes with cationized ferritin (small arrows indicate an area where a small cluster of the small ferritin particles are apparent) in a structure containing MPR (*arrowheads*). (*e*) HRP was internalized from the apical surface and BSA-gold (14 nm) from the basolateral surface for 2 h at 37°C. HRP (labeled with anti-HRP and 9 nm protein A-gold, *small arrows*) colocalizes with internalized BSA-gold (*large arrows*) in compartments containing significant levels of MPR (small gold, *arrowheads*). Anti-HRP labeling is low compared with the labeling from the basolateral surface (compare with Fig. 4, *c* and *d*) but significantly above background. Bars, 0.1 μm.

at 37°C. Stereological analysis was then performed to determine the volume density (or volume fraction) of the labeled compartments (Table II).

After 5 min of basolateral uptake of HRP, reaction product was visualized within tubulovesicular organelles located close to the lateral and basal surfaces of the cells, as described above. The volume density of the labeled structures at this time was 0.34 ± 0.05% of the cytoplasmic volume.[2]

A 10-min incubation resulted in a similar labeling pattern with no significant increase in the volume density of the labeled compartment (0.40 ± 0.04%). To determine whether any HRP had reached late endosomes at this time and to define more accurately the volume of the basolateral early endosome, we stained cells for acid phosphatase after internalization of HRP for 10 min at 37°C. The diffuse reaction product in the HRP-labeled structures was readily distinguishable from the electron-dense, acid phosphatase–positive structures. The HRP-labeled acid phosphatase–negative compartment, which we defined as the early endosome, had a volume density of 0.37 ± 0.05%, not significantly smaller than the total HRP-labeled compartment at this time.

After a 5-min incubation with HRP in the apical medium,

2. The electron-lucent parts of these structures were assumed to be HRP negative and only the HRP-reactive area surrounding these regions was included in the analysis (Fig. 1 *a* and Griffiths et al., 1989*a*). However, as shown in the legend to Table III, our basic conclusions are unchanged if the electron-lucent areas of the structures are also assumed to be part of the early endosomal compartment.

Table I. Distribution of Colloidal Gold Particles within the MDCK Cell after a 40-min Basolateral Incubation and a 40-min or Overnight Chase at 37°C

	40-Min chase	Overnight chase
Estimated No. of gold particles per cell (± SEM)*	4,950 ± 1,390	5,270 ± 2,040
Percentage (and estimated no. per cell) of internalized gold particles‡ in (*a*) MPR +ve strs	75 (3,710)	27 (1,420)
(*b*) MPR −ve strs	25 (1,240)	73 (3,850)
No. of labeled structures per unit cytoplasmic volume (± SEM)§	9 ± 1	3 ± 1
Mean no. of gold particles in labeled profile (± SEM)§	7 ± 2	24 ± 7
Percentage of gold particles in basal region of cell (± SEM)§	31 ± 14	4 ± 3

* Data obtained from analysis of 27 micrographs of Epon sections, final magnification 41,000×. Sections were assumed to be of a uniform thickness of 60 nm to gain estimates for the number of gold particles internalized per cell (volume 1,163 μm^3).

‡ Data obtained by labeling frozen sections of the same experiment with anti-MPR antibodies. Any profiles containing internalized gold were scored as MPR positive (i.e., containing three or more MPR-directed gold particles) or MPR negative. 120 structures were examined after the 40-min chase and ~60 min after the overnight chase (i.e., for each time point the distribution of over 1,600 gold particles was assessed) and the experiment was performed three times. The percentage of internalized gold particles within MPR positive structures varied by ~15% between these experiments. From the estimated number of gold particles per cell in these compartments (shown in parentheses), it is evident that the decrease in the number of gold particles in the MPR compartment (≈2,300) is similar to the increase in the number of particles in lysosomes (≈2,600).

§ Estimates from analysis of micrographs of Epon sections as above. The basal region of the cell was defined as the portion of the cell basal to the midpoint of the nucleus.

few HRP-labeled structures were evident (a volume density of 0.02 ± 0.01%). As described above, a number of small uncoated vesicles or tubules of a similar size to coated vesicles directly underlying the apical surface were labeled (Fig. 1 *c*). Serial-section analysis showed that these structures were not part of the larger tubulovesicular early endosomes (results not shown). After 10 min of HRP internalization at 37°C, more of the larger tubulovesicular structures were labeled (Fig. 1 *a*) and the volume density increased fivefold to 0.11 ± 0.03%. The volume density of the HRP-labeled acid phosphatase-negative compartment at this time was 0.10 ± 0.03%, showing that little HRP had been delivered to acid phosphatase-positive compartments.

After 15 min of endocytosis at 37°C from the basolateral surface, HRP could be detected in juxtanuclear acid phosphatase-positive structures (results not shown) and the volume density increased to 0.72 ± 0.08% of the cytoplasmic volume. Similarly, between 10 and 15 min of uptake from the apical surface, the volume density almost doubled from 0.11 to 0.18 ± 0.05% of the cytoplasmic volume.

At later times of internalization the volume density of structures labeled from both surfaces gradually increased, reaching 2.28 ± 0.21% of the cytoplasmic volume after 2 h uptake from the basolateral surface, and 1.07 ± 0.17% after the same period of uptake from the apical surface. After 2 h of uptake, the number of labeled structures surrounding the nucleus had visibly increased, and in the case of basolateral uptake, a row of small tubular or vesicular structures directly underlying the apical surface were apparent. These structures appear to be distinct from apical early endosomes (results not shown). Such structures have been described previously (von Bonsdorff et al., 1985; Hoppe et al., 1985) and may be involved in transcytosis.

To ascertain the volume of the later compartments in the two endocytic pathways, cells were incubated either apically or basolaterally with HRP for 2 h, washed, and incubated for a further 2 h in HRP-free medium. After the chase period, the typical labeling of the apical and basolateral early endosomes was no longer apparent. The structures labeled from the two surfaces appeared similar, although labeling of the subapical structures described above was only evident after basolateral addition of HRP. The quantitative data showed that the structures labeled from the basolateral side occupied approximately twice the volume of those labeled after apical administration (1.78 ± 0.23 vs. 0.93 ± 0.13% of the cytoplasmic volume).

To investigate further the volume of the late compartments accessible to apical and basolateral ligands, two approaches were taken. Firstly, we measured the volume density of the acid phosphatase-positive compartment (i.e., late endosomes and lysosomes) in the MDCK cell. Secondly, we administered HRP simultaneously to the two surfaces of the MDCK cell. We then investigated whether the volume density of structures labeled in this way was equal to the sum of the volume densities of structures labeled from the two surfaces independently.

After staining for acid phosphatase, reaction product was evident within mostly circular or oval-profiled structures that were predominantly positioned around the cell nucleus. Internal membrane structures were sometimes apparent within these profiles, which appeared very similar to those seen in the MPR-enriched late endosomes and lysosomes. The volume density of acid phosphatase-reactive structures was 1.44 ± 0.21% of the cytoplasmic volume, not significantly different from the volume of structures labeled by basolateral HRP after a 2-h incubation followed by a 2-h chase. The total combined volumes of the late endosomes and lysosomes, defined as acid phosphatase-positive, thus appeared to be similar to the volume of those late compartments accessible to basolateral ligands. When HRP was internalized from both surfaces for 2 h and then chased for a further 2 h, the total volume density of the structures labeled in this way (1.74 ± 0.21%) was, again, not significantly different from that of the compartment labeled only from the basolateral side. This makes it unlikely that there is a major class of late structures accessible only to apically endocytosed ligands, but a subclass of structures only labeled by basolaterally administered markers may exist.

Estimates of the absolute volumes and surface areas of the endocytic compartments per MDCK cell, as well as some morphometric features of the cell, are given in Table III. From these estimates it is apparent that the basolateral early endosomes are ~3.5 times larger in volume and in surface area than the apical early endosomes. This is similar to the ratio of the areas of the two surface domains (3.8 ± 0.5:1).[3]

3. This ratio is significantly lower than that estimated by von Bonsdorff et al. (1985; 7.6:1). This difference can be explained by variations in the type of filter used as well as in the precise growth conditions, both of which can affect the final appearance of the MDCK cells (unpublished observations).

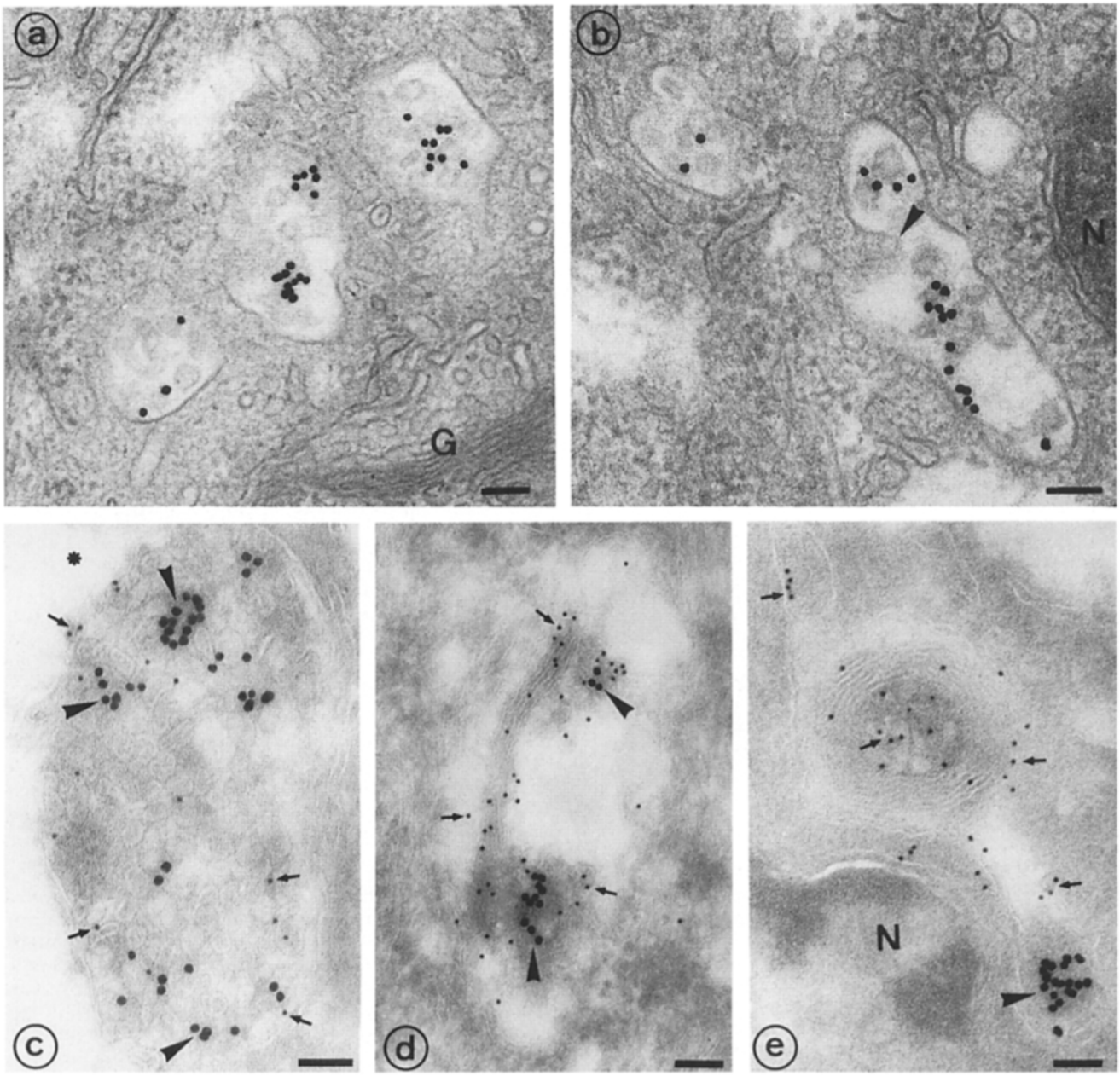

Figure 6. Late endosomes (prelysosomes) of the MDCK cell. *a* and *b* show Epon sections of typical structures labeled with internalized BSA-gold after a 40-min incubation in the basolateral medium at 37°C and a 40-min chase in marker-free medium. The labeled structures are located close to the Golgi (*G*) and nucleus (*N*). Numerous internal vesicular profiles are evident. These may not all be free vesicles but simply infoldings of the limiting membrane as indicated by the arrowhead in *b*. *c*, *d*, and *e* show cryosections from the same experiment as above labeled with anti-MPR and protein A-gold. Internalized basolaterally administered gold (large particles, *arrowheads*) are located within structures containing relatively high levels of MPR (small gold, *arrows*). Internal membranes are evident within all the labeled structures and appear as circular profiles (e.g., *c* and *d*) or as myelin-like arrays of parallel membranes (*d* and *e*). In *e*, the MPR and internalized gold appear to be segregated to different areas of the same structure. *N*, nucleus. In *c*, an asterisk indicates an area of the cell that most likely contained glycogen deposits. These are invariably not retained in our routine frozen sections leaving large "empty" areas. Bars, 0.1 μm.

Discussion

In the preceding paper (Bomsel et al., 1989) a combined biochemical and confocal microscopic approach was used to investigate the spatial organization of the endocytic apparatus in polarized monolayers of MDCK cells and to demonstrate meeting of the apical and basolateral pathways of endocytosis. In this paper, we used an ultrastructural approach to carry out a detailed characterization of the endocytic pathways and in particular to identify the compartment where meeting occurs. In addition, we have obtained estimates for the volumes and surface areas of the endocytic compartments. We were able to distinguish three distinct endocytic structures in the MDCK cell: peripherally located early endosomes, perinuclear late endosomes, and lysosomes.

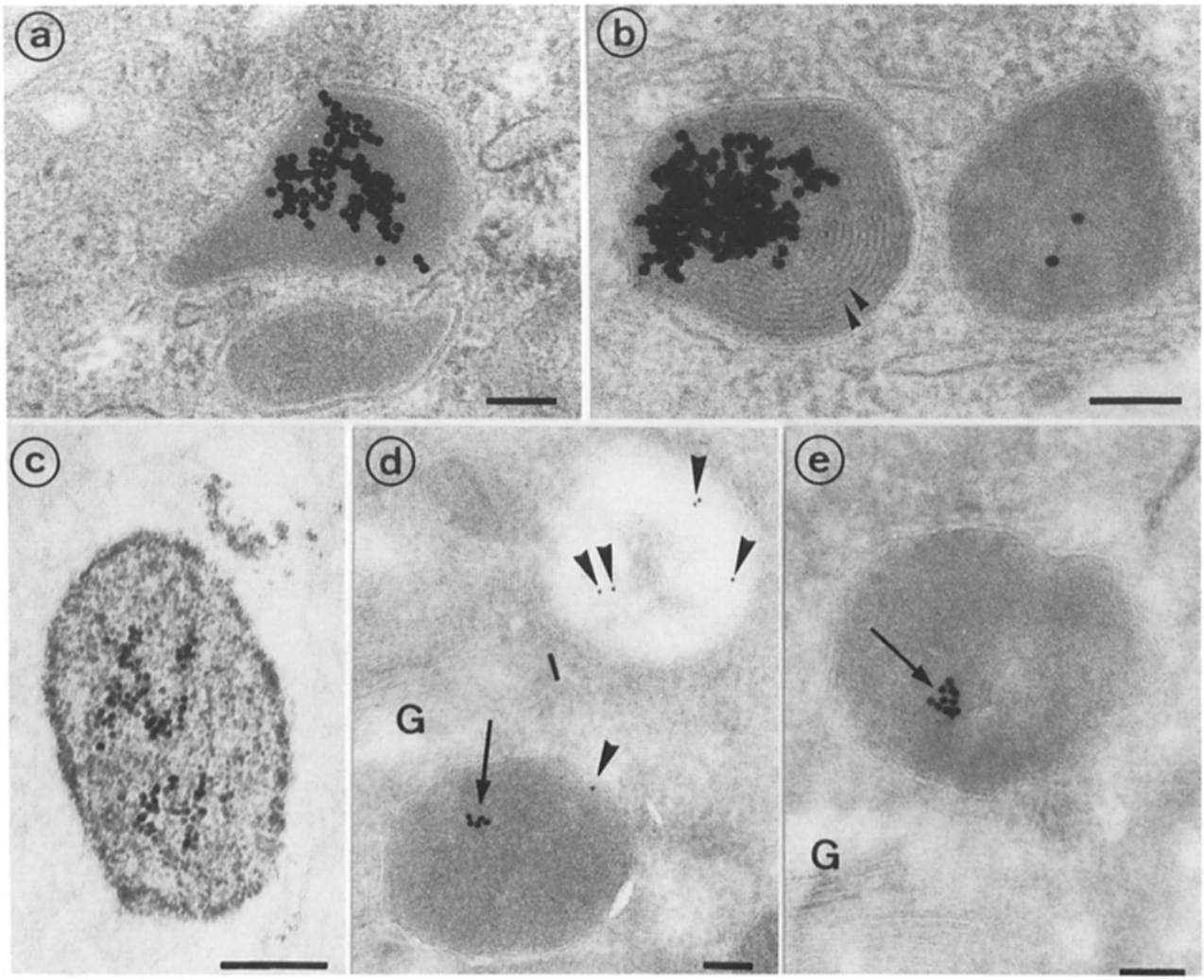

Figure 7. Putative lysosomes of the MDCK cell. *a*, *b*, and *c* show typical structures labeled with BSA-gold after a 40-min incubation in the basolateral medium at 37°C and an overnight chase in marker-free medium. Large aggregates of gold particles are present within the electron-dense lumen of the labeled structures (*a* and *b*) (compare with Fig. 7, *a* and *b*). Parallel arrays of membranes were often observed (e.g., *b*, *arrowheads*). *c* shows an unstained section of a parallel experiment in which the cells were reacted for acid phosphatase after fixation. Despite some background cytoplasmic reaction product, the gold-labeled structure is clearly acid phosphatase-positive. *d* and *e* show cryosections labeled with anti-MPR antibodies. The electron-dense structures containing internalized gold (large gold, *arrows*) do not have significant levels of MPR (small gold, *arrowheads*). In *d*, an adjacent profile is evident that labels significantly for MPR but is free of the internalized gold. *G*, Golgi. Bars, 0.1 μm.

Table II. Summary of Volume Density Measurements

	Time	Volume density	
		Apical medium	Basolateral medium
	min	*% of cytoplasmic volume ± SEM*	
HRP	5	0.02 ± 0.01	0.34 ± 0.05
	10	0.11 ± 0.03	0.40 ± 0.04
	10	0.10 ± 0.03	0.37 ± 0.06
	(AP^-)§		
	15	0.18 ± 0.05	0.72 ± 0.08
	30	0.32 ± 0.06	1.22 ± 0.10
	60	0.66 ± 0.09	1.68 ± 0.22
	120	1.07 ± 0.17	2.28 ± 0.21
	120 plus 120 chase	0.93 ± 0.13	1.78 ± 0.23
Acid phosphatase		1.74 ± 0.14*	
		1.44 ± 0.21‡	

* HRP in apical and basolateral medium.
‡ Measurements were restricted to vesicular compartments (diameter > 50 nm) to exclude the Golgi stacks and TGN, which showed variable acid phosphatase activity as in other cell types (see Hand and Oliver, 1984; Griffiths and Simons, 1986).
§ HRP-labeled acid phosphatase-negative structure.

Table III. Summary of Volume and Surface Area Estimates for the MDCK I Cell

	Value ± SEM
Cell volume	1,163 ± 200 μm^3
Cytoplasmic volume	955 ± 184 μm^3
Apical membrane area	478 ± 102 μm^2
Basolateral membrane area	1,798 ± 341 μm^2
Basolateral/apical area ratio	3.8 ± 0.5 μm^2
Apical early endosome*	
Volume per cell	0.96 ± 0.34 μm^3
Absolute surface per cell	48 ± 17 μm^2
Basolateral early endosome*	
Volume per cell	3.53 ± 0.88 μm^3
Absolute surface per cell	152 ± 39 μm^2
Late endosomes and lysosomes‡	
Volume per cell	13.8 ± 3.3 μm^3
Absolute surface per cell	248 ± 72 μm^2

* Calculated from the volume density measurements for acid phosphatase-negative structures labeled with HRP after a 10-min apical or basolateral incubation at 37°C. For these measurements, HRP limited to the periphery of a structure was assumed to be in a tubule surrounding an electron-lucent area (see text). If the electron-lucent area is assumed to be part of the early endosomal compartment the corrected values would be as follows: apical early endosome volume = 1.14 ± 0.40 μm^3, surface area = 46 ± 17 μm^2; basolateral early endosome volume = 4.49 ± 1.11 μm^3, surface area = 126 ± 32 μm^2.

‡ Calculated from the volume density of the acid phosphatase-positive compartment.

Early Endosomes

The early endosomes of the MDCK cell were labeled with fluid-phase markers after short incubations (5–10 min) at 37°C. These structures showed low or negligible labeling for MPR and did not contain detectable amounts of acid phosphatase. In agreement with the confocal microscopic results of Bomsel et al. (1989), our electron microscopic studies have shown that there are two distinct sets of early endosomes in the MDCK cell that receive material only from the adjacent surface domain. The basolateral early endosomes were located very close to the basolateral surface of the cell and the apical early endosomes were shown to lie between the Golgi complex and the apical cell surface.

Although the structure of the apical and basolateral early endosomes was fairly similar, with both containing tubular and vesicular elements, they differed somewhat in their kinetics of filling. The volume of the basolaterally labeled compartment showed no change between 5 and 10 min of incubation at 37°C as previously shown for macrophages and L cells (Steinman et al., 1976) and for baby hamster kidney cells (Griffiths et al., 1989*a*). In contrast, the volume of the apically labeled compartment showed a fivefold increase over the same time period. This delay in filling the apical early endosome may be indicative of a slower passage of clathrin-coated or uncoated vesicles between the apical cell surface and the apical early endosomes; after 5 min, insufficient HRP may have been delivered to these structures to reach the threshold concentration necessary for detection. Our observation of HRP-labeled uncoated vesicles underlying the apical surface after short periods of internalization is consistent with this interpretation. Whether there exists some filamentous network analogous to (although less extensive than) the terminal web of the brush border, which retards the movement of these vesicles is unknown at present.

How the apical and basolateral early endosomes are kept distinct is not clear. Recent studies have shown that one of the most striking characteristics of early endosomes in vitro is their tendency to fuse rapidly and efficiently with each other (Gruenberg and Howell, 1987; Braell, 1987; Diaz et al., 1988). Clearly, few of the apical and basolateral endosomes of MDCK cells fuse with one another in vivo or mixing of their content would be observed. This could be due to the two classes of endosomes lacking the competence to fuse with one another or, alternatively, they may simply be kept spatially separate by cytoskeletal elements.

The importance of maintaining the distinct apical and basolateral early endosomes is shown by the functional characterization of the endocytic pathways presented in the preceding companion paper (Bomsel et al., 1989). Sorting of fluid to transcytosis and recycling was shown to be mediated mainly by the early endosomes underlying the two surface domains. There was no evidence for later compartments having a major role in recycling or transcytosing the internalized marker. The separation of the endocytic pathways at the level of the early endosome thus ensures that no mixing of components from the apical and basolateral surface domains occurs before sorting takes place, and that the two sets of endosomes must only deal with incoming material from one surface.

The apical early endosomes are estimated to occupy 0.10% of the cytoplasmic volume, an absolute volume of 0.96 μm^3 per cell, and to have a surface area of 53 μm^2 per cell. The apical endosomes are therefore approximately three to four times smaller in volume and in surface area than the basolateral early endosomes, a volume of 3.53 μm^3, and surface area of 152 μm^2. This ratio is similar to the ratio of the surface areas of the two surface domains (apical-to-basolateral ratio 1:3.8) and to the total endocytic rate from the two domains (1:3.6, Bomsel et al., 1989). The size of the early endosomal compartment thus may be related to the total constitutive endocytic uptake from the surface, which in turn depends on the surface area available for endocytosis.

Late Endosomes and Lysosomes

After 15 min at 37°C, fluid-phase markers internalized independently from the two surfaces of MDCK cells met in a perinuclear endosomal compartment. Meeting of the apical and basolateral endocytic pathways in other polarized cells has previously been demonstrated, but the compartments shared by the two pathways were not characterized. Meeting of basolateral and apical markers was shown to occur in isolated proximal tubules after 30 min of perfusion (Nielsen et al., 1985), but meeting was ascribed to a minor pathway in the cell; the majority of labeled vesicles contained only one of the two tracers even after a further 2-h chase. Meeting of basolateral and apical markers was also shown in pancreatic acinar cells but only after 4–5 h of tracer administration and within apically located structures, which were considered to be lysosomes (Oliver, 1982).

The endosomes in MDCK cells where meeting occurred were shown to be enriched in MPR and were located in a perinuclear position. These structures resembled multivesicular bodies and showed similar morphological characteristics to the MPR-enriched late endosomal or prelysosomal compartment recently described in normal rat kidney cells (Griffiths et al., 1988) and therefore we term these structures

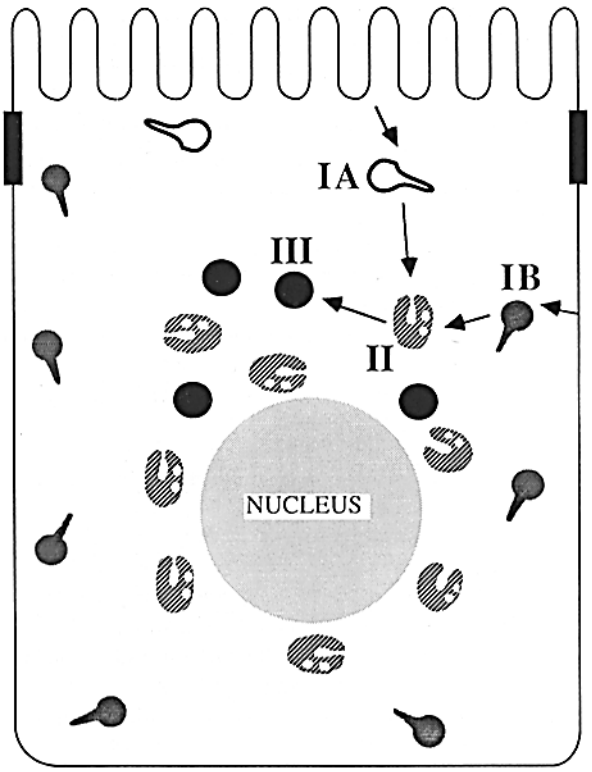

Figure 8. Schematic diagram of the endocytic pathways in the MDCK cell. Internalized material from the two surface domains first enters two distinct classes of peripherally located early endosomes; the apical early endosomes (*IA*) and the basolateral early endosomes (*IB*). The two pathways meet in a late endosomal or prelysosomal compartment (*II*) enriched in MPR. For simplicity, only one of the late endosomes is shown receiving internalized material from the two domains, but colocalization of apical markers was observed even in structures basal to the nucleus. Finally, internalized material passes to the lysosomes (*III*) that appear to be predominantly in the apical portion of the cell.

late endosomes (Kornfeld and Mellman, 1989). As in normal rat kidney cells (Griffiths G., R. Matteoni, R. Back, and B. Hoflack, manuscript in preparation), these structures show reactivity for acid phosphatase. This compartment has also been shown to have detectable amounts of β-glucuronidase, cathepsin D, and a significant concentration of the lysosomal membrane glycoprotein, lgp 120 (Griffiths et al., 1988). The presence of these lysosomal markers, as well as MPR and internalized ligands, have led to its proposed role as an intermediate compartment where the MPR releases its cargo of newly synthesized lysosomal enzymes from the TGN before the MPR recycles back to the Golgi complex. Clearly this compartment must have a role in sorting MPR from endocytosed components en route to lysosomes. In the MDCK cell, the two endocytic pathways bringing components destined for degradation meet in this compartment, but sorting of ligands for recycling or transcytosis has presumably been performed by early endosomes before this mixing occurs.

The late endosomes in MDCK cells are predominantly located in the Golgi area, but are also observed in basal areas of the cell. This distribution does not appear to reflect functional variations within the late endosome population in that both apical and basolateral ligands were observed in these structures in all regions of the cell. There appear to be no late endocytic structures (late endosomes and lysosomes) labeled from the apical surface that are not accessible to basolaterally administered ligands. On the other hand, there may be late structures only accessible to basolaterally internalized ligands, as basolaterally labeled structures occupied twice the volume of those labeled from the apical side. However, we feel that a more likely explanation for these results is that apical HRP does not reach the threshold for detection in all the late structures to which it can be delivered. As shown in the preceding paper (Bomsel et al., 1989), the fraction of an internalized marker passing from early endosomes to late compartments is much smaller for the apical pathway than for the basolateral pathway; 90% of the fluid in the apical early endosome is released through transcytosis and recycling. The small amount of HRP that reaches the late endosomes may be significantly diluted and so may not be detected in all these structures.

The end stations for endocytosed ligands in the MDCK cell are the MPR-negative, acid phosphatase–reactive lysosomes. Internalized gold particles accumulated within these structures after passing through the MPR-enriched late endosomes, as shown by quantitation of the gold particles in the two compartments before and after an overnight chase. The kinetics of transfer to the lysosomes cannot be inferred from these data because gold particles may be retarded in their transport as compared to other markers (cf. Bomsel et al., 1989). The late endosomes and lysosomes together occupy 1.44% of the cytoplasmic volume, an absolute volume of 13.8 μm^3, and have a surface area of 248 μm^2 per cell (excluding internal membranes). The lysosomal compartment appears to be smaller in volume than the late endosome; approximately half as many labeled profiles per cell were evident after the overnight chase as compared with the 40-min chase, and the number of gold particles per profile was significantly higher.

Morphologically, lysosomes showed some similarities in structure to the late endosomes but vesicular membrane contents were rarely observed and the lumen of the lysosomes appeared more condensed and electron dense. Myelin-like arrays of membranes were, however, often observed in lysosomes. The lysosomes showed a different spatial distribution in the cell to the late endosomes, being almost exclusively located in the apical half of the cell. The functional significance of this organization is unknown at present. However, preliminary observations on MDCK cells have suggested that the late endosomes may be a highly dynamic compartment. These structures move apically or basally upon changing the intracellular pH (Parton, R., G. R. Bacallao, K. Simons, and K. Prydz, manuscript in preparation), consistent with results in nonpolarized cells (Heuser, 1989).

Conclusions

It is apparent that the endocytic pathway shows a very high degree of spatial organization within the MDCK cell (as summarized in Fig. 8). The two distinct sets of early endosomes, functionally defined as mediating recycling and transcytosis, are located peripherally in the cell. The pathways from these early endosomes to the lysosomes converge at the level of the MPR-enriched late endosomes or prelysosomes located all around the nucleus. Ligands finally accumulate within apically located MPR-negative lysosomes. This orga-

nization is in marked contrast to the organization of the endocytic apparatus of MDCK cells grown on an impermeable plastic support. Matlin et al. (1983) showed that a marker for the apical surface appeared within endocytic structures distributed throughout the whole cell after just a few minutes of internalization at 37°C. These differences may well reflect the lower degree of organization of cytoskeletal elements (particularly microtubules) within the plastic-grown cell as compared with the filter-grown cell. Filter-grown MDCK cells show a distinct pattern of microtubules, with 90% of the microtubules that run vertically through the cell having the same polarity (Bacallao et al., 1989). This specialized organization may well prove to be important in directing membrane traffic in the polarized cell during both endocytosis and exocytosis.

The calculated total uptake rates for the two surface domains of the MDCK cell (Bomsel et al., 1989) correspond to the internalization of ~120 vesicles (internal diameter, 100 nm; volume, $5 \times 10^{-4}\ \mu m^3$) from the apical surface per minute per cell and 440 vesicles per minute from the basolateral surface. On this basis, one cell would internalize ~0.7% of the area of each plasma membrane surface per minute. Thus, an area of plasma membrane equivalent to each surface domain would be internalized in ~2.5 h. When one considers this flow of membrane into the cell and the constant transcytosis between the two domains (equivalent to ~60 100-nm-diam vesicles per minute per cell in each direction), it is clear that very efficient sorting mechanisms must exist to maintain the distinct composition of the two domains. Clearly, the MDCK cell system will be a useful model system to study these mechanisms.

Special thanks are due to Jean Gruenberg for numerous helpful discussions and for advice about the manuscript. We would also like to thank John Tooze for comments on the manuscript; Hilkka Virta for help with cell culture; Ruth Back for technical assistance; and Helen Fry for efficient secretarial work. Transwell filters were kindly provided by H. Lane (Costar Corp., Cambridge, MA).

R. G. Parton was a recipient of long-term Royal Society and European Molecular Biology Organization (EMBO) fellowships; K. Prydz was a recipient of a long-term fellowship from the National Council of Science and Humanities (NAVF), Norway; and M. Bomsel was a recipient of a one-year EMBO fellowship.

Received for publication on 16 June 1989 and in revised form 18 September 1989.

References

Abrahamson, D. R., and R. Rodewald. 1981. Evidence for the sorting of endocytic vesicle contents during the receptor-mediated transport of IgG across the newborn rat intestine. *J. Cell Biol.* 91:270–280.

Bacallao, R., C. Antony, C. Dotti, E. Karsenti, E. H. K. Stelzer, and K. Simons. 1989. The subcellular organization of MDCK cells during the formation of a polarized epithelium. *J. Cell Biol.* 109:2817–2832.

Baddeley, A. J., H. J. G. Gundersen, and L. M. Cruz-Orive. 1986. Estimation of surface areas from vertical sections. *J. Microsc. (Oxford).* 142:259–276.

Bomsel, M., K. Prydz, R. G. Parton, J. Gruenberg, and K. Simons. 1989. Endocytosis in filter-grown Madin–Darby canine kidney cells. *J. Cell Biol.* 109:3243–3258.

Braell, W. A. 1987. Fusion between endocytic vesicles in a cell-free system. *Proc. Natl. Acad. Sci. USA.* 84:1137–1141.

Brown, W. J., J. Goodhouse, and M. G. Farquhar. 1986. Mannose 6-phosphate receptors for lysosomal enzymes cycle between the Golgi complex and endosomes. *J. Cell Biol.* 103:1235–1247.

Courtoy, P. 1989. Dissection of endosomes. *In* Intracellular Trafficking of Proteins. C. Ster and J. Cianover, editors. Cambridge University Press, NY. In press.

Cruz-Orive, L. M., and E. G. Hunziker. 1986. Stereology of anisotropic cells: application to growth cartilage. *J. Microsc. (Oxford).* 143:47–80.

de Chastellier, C., T. Lang, A. Ryter, and L. Thilo. 1987. Exchange kinetics and composition of endocytic membranes in terms of plasma membrane constituents: a morphometric study in macrophages. *Eur. J. Cell Biol.* 44: 112–113.

Diaz, R., L. Mayorga, and P. Stahl. 1988. *In vitro* fusion of endosomes following receptor-mediated endocytosis. *J. Biol. Chem.* 263:6093–6100.

Dunn, W. A., A. L. Hubbard, and N. N. Aronson. 1980. Low temperature selectively inhibits fusion between pinocytic vesicles and lysosomes during heterophagy of ^{125}I-asialofetuin by perfused rat liver. *J. Biol. Chem.* 255:5971–5978.

Fuchs, R., S. Schmid, and I. Mellman. 1989. A possible role for Na^+,K^+-ATPase in regulating ATP-dependent endosome acidification. *Proc. Natl. Acad. Sci. USA.* 86:539–543.

Fuller, S. D., and K. Simons. 1986. Transferrin receptor polarity and recyling accuracy in "tight" and "leaky" strains of Madin-Darby canine kidney cells. *J. Cell Biol.* 103:1767–1779.

Fuller, S., C.-H. von Bonsdorff, and K. Simons. 1984. Vesicular stomatitis virus infects and matures only through the basolateral surface of polarized epithelial cell line, MDCK. *Cell.* 38:65–77.

Geuze, H. J., J. W. Slot, G. J. A. M. Strous, H. F. Lodish, and A. L. Schwartz. 1983. Intracellular site of asialoglycoprotein receptor-ligand uncoupling: double-label immunoelectron microscopy during receptor-mediated endocytosis. *Cell.* 32:277–287.

Geuze, H. J., W. Stoorvogel, G. J. Strous, J. W. Slot, J. E. Bleekemolen, and I. Mellman. 1988. Sorting of mannose-6-phosphate receptors and lysosomal membrane proteins in endocytic vesicles. *J. Cell Biol.* 107:2491–2501.

Goda, Y., and S. R. Pfeffer. 1988. Selective recycling of the mannose-6-phosphate/IGF-11 receptor to the trans Golgi network in vitro. *Cell.* 55:309–320.

Goldstein, J. L., M. S. Brown, R. G. W. Anderson, D. W. Russel, and W. J. Schneider. 1985. Receptor mediated endocytosis: concepts emerging from the LDL receptor system. *Annu. Rev. Cell Biol.* 1:1–39.

Griffiths, G., R. Back, and M. Marsh. 1989*a*. A quantitative analysis of the endocytic pathway in baby hamster kidney cells. *J. Cell Biol.* 109:2703–2720.

Griffiths, G., S. D. Fuller, R. Back, M. Hollinshead, S. Pfeiffer, and K. Simons. 1989*b*. The dynamic nature of the Golgi complex. *J. Cell Biol.* 108:277–297.

Griffiths, G., B. Hoflack, K. Simons, I. Mellman, and S. Kornfeld. 1988. The mannose-6-phosphate receptor and the biogenesis of lysosomes. *Cell.* 52:329–341.

Griffiths, G., K. Simons, G. Warren, and K. T. Tokuyasu. 1983*a*. Immunoelectron microscopy using thin, frozen sections: applications to studies of the intracellular transport of Semliki Forest virus spike glycoproteins. *Methods Enzymol.* 96:435–450.

Griffiths, G., P. Quinn, and G. Warren. 1983*b*. Dissection of the Golgi complex. I. Monensin inhibits the transport of viral proteins from medial to *trans* Golgi cisternae in baby hamster kidney cells infected with Semliki forest virus. *J. Cell Biol.* 96:835–850.

Griffiths, G., and K. Simons. 1986. The trans Golgi network: sorting at the exit site of the Golgi complex. *Science (Wash. DC).* 234:438–443.

Griffiths, G., G. Warren, P. Quinn, O. Mathieu-Costello, and H. Hoppeler. 1984. Density of newly-synthesized plasma membrane proteins in intracellular membranes. I. Stereological studies. *J. Cell Biol.* 98:2133–2141.

Gruenberg, J., G. Griffiths, and K. E. Howell. 1989. Characterization of the early endosome and putative endocytic carrier vesicles in vivo and with an assay of vesicle fusion in vitro. *J. Cell Biol.* 108:1301–1316.

Gruenberg, J., and K. E. Howell. 1987. An internalized transmembrane protein resides in a fusion-competent endosome for less than 5 minutes. *Proc. Natl. Acad. Sci. USA.* 84:5758–5762.

Gruenberg, J., and K. E. Howell. 1989. Membrane traffic in endocytosis: insights from cell-free assays. *Annu. Rev. Cell Biol.* In press.

Hand, A. R., and C. Oliver. 1984. The rôle of GERL in the secretory process. *In* Cell Biology of the Secretory Process. M. Cantin, editor. Karger Press, Basel, Switzerland. 148–170.

Helenius, A., I. Mellman, D. Wall, and A. Hubbard. 1983. Endosomes. *Trends Biochem. Sci.* 8:245–250.

Heuser, J. 1989. Changes in lysosome shape and distribution correlated with changes in cytoplasmic pH. *J. Cell Biol.* 108:855–864.

Hopkins, C. R. 1986. Membrane boundaries involved in the uptake and intracellular processing of cell surface receptors. *Trends Biochem. Sci.* 11:473–477.

Hopkins, C. R., and I. S. Trowbridge. 1983. Internalization and processing of transferrin and the transferrin receptor in human carcinoma A431 cells. *J. Cell Biol.* 97:508–521.

Hoppe, C. A., T. P. Connolly, and A. L. Hubbard. 1985. Transcellular transport of polymeric IgA in the rat hepatocyte: biochemical and morphological characterization of the transport pathway. *J. Cell Biol.* 101:2113–2123.

Hubbard, A. L. 1989. Endocytosis. *Curr. Op. Cell Biol.* 1:675–683.

Kornfeld, S., and I. Mellman. 1989. The biogenesis of lysosomes. *Annu. Rev. Cell Biol.* In press.

Limet, J. N., J. Quintart, Y.-J. Schneider, and P. J. Courtoy. 1985. Receptor-mediated endocytosis of polymeric IgA and galactosylated serum albumin in rat liver. *Eur. J. Biochem.* 146:539–548.

Marsh, M., E. Bolzau, and A. Helenius. 1983. Penetration of Semliki Forest virus from acidic prelysosomal vacuoles. *Cell.* 32:931–940.

Marsh, M., G. Griffiths, G. E. Dean, I. Mellman, and A. Helenius. 1986. Three-dimensional structure of endosomes in BHK-21 cells. *Proc. Natl. Acad. Sci. USA.* 83:2899–2903.

Matlin, K., D. F. Bainton, M. Pesonen, D. Louvard, N. Genty, and K. Simons. 1983. Transepithelial transport of a viral membrane glycoprotein implanted into the apical plasma membrane of Madin-Darby Canine Kidney cells. I. Morphological evidence. *J. Cell Biol.* 97:627–637.

McKanna, J. A., H. T. Haigler, and S. Cohen. 1979. Hormone receptor topology and dynamics: morphological analysis using ferritin-labeled epidermal growth factor. *Proc. Natl. Acad. Sci. USA.* 76:5689–5693.

Mostov, K. E., and N. E. Simister. 1985. Transcytosis. *Cell.* 43:389–390.

Nielsen, J. T., S. Nielsen, and E. I. Christensen. 1985. Transtubular transport of proteins in rabbit proximal tubules. *J. Ultrastruct. Res.* 92:133–145.

Oliver, C. 1982. Endocytic pathways at the lateral and basal cell surfaces of exocrine acinar cells. *J. Cell Biol.* 95:154–161.

Schmid, S., R. Fuchs, M. Kielian, A. Helenius, and I. Mellman. 1989. Acidification of endosome subpopulations in wild-type chinese hamster ovary cells and temperature-sensitive acidification-defective mutants. *J. Cell Biol.* 108: 1291–1300.

Simons, K., and S. D. Fuller. 1985. Cell surface polarity in epithelia. *Annu. Rev. Cell Biol.* 1:243–288.

Slot, J. W., and H. J. Geuze. 1985. A novel method to make gold probes for multiple labeling cytochemistry. *Eur. J. Cell Biol.* 38:87–93.

Steinman, R. M., S. E. Brodie, and Z. A. Cohn. 1976. Membrane flow during pinocytosis. A stereologic analysis. *J. Cell Biol.* 68:665–687.

Steinman, R. M., I. S. Mellman, W. A. Muller, and Z. A. Cohn. 1983. Endocytosis and the recycling of plasma membrane. *J. Cell Biol.* 96:1–27.

Storrie, B. 1988. Assembly of lysosomes: perspectives from comparative molecular cell biology. *Int. Rev. Cytol.* 111:53–105.

von Bonsdorff, C.-H., S. D. Fuller, and K. Simons. 1985. Apical and basolateral endocytosis in Madin-Darby canine kidney (MDCK) cells grown on nitrocellulose filters. *EMBO (Eur. Mol. Biol. Organ.) J.* 4:2781–2792.

Wall, D. A., G. Wilson, and A. L. Hubbard. 1980. The galactose-specific recognition system of mammalian liver: the route of ligand internalization in rat hepatocytes. *Cell.* 21:79–93.

Weibel, E. R. 1979. Stereological Methods. 1. Practical methods for biological morphometry. Academic Press, Inc., NY.